Chain-based Collision Avoidance for UAS Sense-and-Avoid Systems

Laith R. Sahawneh* and Randal W. Beard †

Brigham Young University, Provo, Utah, 84602, USA

Sharath Avadhanam‡ and He Bai ‡

UtopiaCompression Corporation, Los Angeles, 90064, USA

An Unmanned Aircraft System (UAS) collision avoidance algorithm for the Sense and Avoid (SAA) problem is proposed. The avoidance path is modeled using a physical analogy of a chain placed in a force field. This approach has the advantage that it continuously searches the space for a proper evasive maneuver to avoid an impending collision with detected intruding aircraft while observing the standard flight rules followed by manned aircraft. The algorithm also accounts for the uncertainties associated with the intruder aircraft's state estimates computed by the detection algorithm. To examine the proposed avoidance algorithm we combined the electro-optical (EO) based Monocular Maneuverless PAssive Ranging System (M2PARS) technology developed by UtopiaCompression Corporation (UC) for detecting imminent collisions using passive imaging sensors and simulated the integrated model to predesigned encounter geometry scenarios in the Matlab/Simulink environment.

I.   INTRODUCTION

The need for a robust SAA system also known as Detect, Sense and Avoid (DSA) system is evident from the complex nature of modern air traffic. The current National Airspace System (NAS) has numerous manned users that are required to follow Federal Aviation Administration (FAA) rules and regulations in order assure safety for the users of NAS. To ensure that UAS do not disrupt other airspace users, they must be integrated into the NAS, through the development of detailed and comprehensive rules, standards and regulations that allow for safe and accident-free aviation. Currently UAS are not authorized by the FAA to operate freely in the NAS due to safety and compliance considerations. However, before FAA and civil aviation authorities can approve routine UAS flight operations, UAS must comply with all applicable regulatory requirements for airspace access, foremost among these requirements is what is known as the *"see-and-avoid"* standard.[1,2]

A.   Manned Aviation and current UAS Regulations

As the design of any SAA system must meet the FAA requirements and regulations, an extensive amount of work has been done to study and understand the current manned aviation regulations as a guide to aid in the development and design of SAA that behave as in manned aircraft.

In the United States (U.S.) the aviation regulations, collectively known as Federal Aviation Regulation (FAR), are codified in the Code of Federal Regulations (CFR), Title 14, Chapter I. The CFR along with

---

*Ph.D. student, research assistant, Department of Electrical and Computer Engineering, Brigham Young University.

†Professor, Department of Electrical and Computer Engineering, Brigham Young University, senior member of AIAA.

‡R&D scientist, UtopiaCompression Corporation, 11150 W. Olympic Blvd, STE 820, Los Angeles, CA.

supplementary material like advisory circulars, technical standards orders and manuals such as the Aeronautical Information Manual (AIM) issued by the FAA, define appropriate standards, procedures, and practices to ensure that operators and manufactures are able to establish a minimum level of safety and reliability required for civil aviation.[1,3]

Foremost among aviation regulations are parts for airspace categories and classes $[CFR\,14, Parts\,71-73]$ and general operating and flight rules $[CFR\,14, Part\,91]$, the right-of-way rules operations $[\S91.113]$, aircraft speed $[\S91.117]$, minimum safe altitudes $[\S91.119]$ and Visual Flight Rules (VFR) $[\S91.151-161]$ to name a few, have a crucial impact on the design and development of SAA system that must provide the Equivalent Level of Safety (ELOS) as manned aviation.

While manned aviation is well established, regulations for unmanned aviation are still being developed since UAS technology is still immature and the FAA is adopting a cautious approach. The process of UAS integration into NAS is challenging because of technical problems like communication issues with ground stations, the ATC, and other aircraft.[4] The first efforts towards UAS regulation took place in the early 1990s, when the FAA issued a notice for proposed rules and formed an industry support group. Efforts to regulate and certify UAS have been driven by a rapid growth in technology and also potential UAS markets in military, civilian and public domains.[1,5–8] To date the FAA has not adopted a framework, but with the recent passage of H.R. 658 the FAA must establish clear guidelines to allow UAS access to the NAS by 2015.[9]

B.   Sense and Avoid

Since the beginning of manned flight the primary method for avoiding midair collisions has been the pilot's eye sight. Even with the introduction of radio communication, radar, and air traffic control (ATC), the FAA has maintained the requirement for a pilot to actively search the sky for other airspace users and maneuver to avoid collision. The SAA functionality can, in general, be broken into three sub-functions: sense and track, collision/conflict detection, and avoidance. The main role of the first sub-function is to detect any of the various types of hazards, such as traffic or terrain, and track the motion of the detected object to gain sufficient confidence that the detection is valid. Currently, EO, Infrared (IR), Radar and Light Detection And Ranging (LIDAR also LADAR) are examples of sensors to detect non-cooperative traffic. Non-cooperative traffic means that no data about conflicting traffic is communicated or transmitted to the UAS from the conflicting intruders or from Air Traffic Control (ATC). On the other hand Traffic Alert and Collision Avoidance System (TCAS) and Automatic Dependent Surveillance-Broadcast (ADS-B) are two examples of systems for detecting cooperative intruders. However, not every aircraft that is observed by the sensing system presents a collision or conflict threat. Therefore the collision/conflict detection determines whether an approaching intruder aircraft is on a collision/conflict course or not. Determining the threat level of an intruding aircraft and maneuvering only when necessary is a difficult challenge, but is an important step forward for the SAA community.

While creating a robust system to detect intruder aircraft is an integral piece of the SAA problem, the development of a Collision Avoidance System (CAS) is equally important. If UAS are to be integrated seamlessly alongside piloted aircraft, they must react to collision threats in the same way as a human pilot. In any encounter scenario that occurs, the UAS's avoidance maneuver must conform to the standard flight rules followed by manned aircraft. Additionally, a CAS system should only maneuver to avoid another aircraft when a collision threat exists. Unnecessary course changes limit flight efficiency and may also confuse other airspace users. It might in addition result in conflict with other air traffic.

Once a collision threat has been detected, the CAS must select the proper evasive maneuver observing the right-of-way rules. The essential requirement for the CAS is to perform the avoidance maneuver in such a way that the distance at the closest point of approach (CPA) of the intruder, d_{cpa}, is equal or greater than a minimum required miss distance. It is generally understood that the minimum miss distance is required to be at least 500 feet to 0.5 nautical mile in all directions.[10,11] While, the current manned regulations state that the aircraft must remain *well clear* from the intruder aircraft, the *well clear* boundary defined in manned regulations (*see* $[CFR\,14, \S91.113]$) has no explicit values but varies as a function of UAS and the intruder performance, conflict geometry and relative accelerations. Yet, we can infer that the *well clear* boundary is considered at separation level and not at avoidance level, since it is defined as the state by which two aircraft are separated in such a way they do not initiate a collision avoidance maneuver.[10] However, in this paper our focus is at the avoidance level. In addition, the initiated maneuver must be compatible with the performance of the UAS and once the conflict is resolved the CAS should return the UAS to the original flight path or to a newly assigned flight plan.

American Institute of Aeronautics and Astronautics

This work develops a collision avoidance approach based on a virtual chain placed in a virtual force field. The chain-based concept was initially presented in Ref. 12 to plan a path using a series of connected waypoints. The waypoints serve as the links of a simulated chain. Since the path is represented using waypoints that are a fixed distance apart, it is easy to determine roughly where the UAS will be at any given time. This timing information can be used to prevent collisions and spread out paths when creating plans to avoid multiple UAS.[12]

We limit the development of collision avoidance algorithm to the 2-D plane to conform with the standard flight rules followed by manned aircraft in situations where the aircraft flying in the airspace and not ascending, descending or operating in the vicinity of an airport. In such case the right-of-way rules defined by manned aviation regulations states that when an aircraft has the right-of-way, then the another shall give way to that aircraft and may not pass over, under, or ahead of it unless well clear (see [$CFR\,14,\S91.113$]). In addition, the manned aviation regulations define two main scenarios for which an aircraft may encounter another aircraft, namely converging and approaching head-on. $CFR\,14,\S91.113.d$ states that when aircraft are converging at approximately the same altitude, the aircraft to the other's right has the right-of-way so that the aircraft that does not have the right-of-way shall alter course to the right in a manner it does not pass over, under, or ahead of the another aircraft. For the approaching scenario, $CFR\,14,\S91.113.e$ states that when aircraft are approaching each other head-on, or nearly so, each aircraft shall alter course to the right. Hence, in scenarios where aircraft are not operating in the vicinity of an airport, ascending or descending, the standard flight rules followed by manned aircraft urge on avoidance maneuvers that prevent altitude change.

II.   Chain-Based Collision Avoidance

The method for finding a path that safely avoids intruder aircraft is based on the work of 12–14. Similarly, we model the chain as a collection of unit-mass points constrained to the 2-D plane. Letting $z_i = (x_i, y_i)^T \in \mathbb{R}^2$, $i = 1, 2, ..., N$ be the position of the ith point or node in the chain, the N-link chain is represented by

$$\mathbf{c} = \left[\mathbf{z}_1^T, \mathbf{z}_2^T, \ldots, \mathbf{z}_N^T\right]^T$$

We limit our discussion If the point masses are unconstrained, then by Newton's second law of motion, the unconstrained dynamics equation describing the entire chain motion is given by

$$\ddot{\mathbf{c}} = \mathbf{F} \tag{1}$$

Where $\mathbf{F}$ is the sum of applied forces, which consists of constrained and unconstrained forces.

The unconstrained forces applied to the chain are composed of two forces: the first pushes the chain towards the ownship target, while the second repels the ownship from the intruder observing the right-of-way rules.
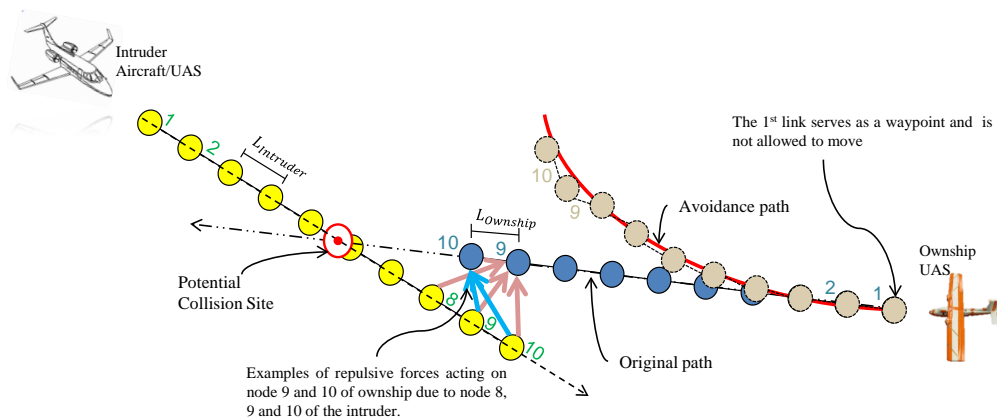

Figure 1. Representation of repulsive forces between chains.

To push the chain in the desired direction it is placed in a force-field that is generated using the gradient of a bounded differential reward function. To create a force that causes the chain of the ownship to avoid

the intruder, first we assume that the position of the ith element in the intruder chain is known. As depicted in Figure 1 let $\mathbf{c}_O = \left[\mathbf{z}_{O1}^T,\ \mathbf{z}_{O2}^T, \ldots, \mathbf{z}_{ON}^T\right]^T$ be the N-link chain associated with the ownship, and let $\mathbf{c}_I = \left[\mathbf{z}_{I1}^T,\ \mathbf{z}_{I2}^T, \ldots, \mathbf{z}_{IN}^T\right]^T$ be the N-link chain associated with the intruder. Note that while both chains have the same number of links the desired distance between each link does not need to be the same for both the ownship and the intruder but should be proportional to speed, so that both chains are associated with a fixed look ahead time T. This implies that each UAS will fly through the ith node in its chain at approximately the same time. Let $\mathbf{d}_{OI}(m, n)$ be the vector from the nth node of the intruder aircraft to the mth node of the ownship UAS, defined as

$$\mathbf{d}_{OI}(m, n) = \mathbf{z}_{Om} - \mathbf{z}_{In} \tag{2}$$

and

$$\hat{\mathbf{d}}_{OI}(m, n) = \frac{\mathbf{d}_{OI}(m, n)}{\|\mathbf{d}_{OI}(m, n)\|}. \tag{3}$$

Where $\| \cdot \|$ is the standard Euclidean norm. As shown in Figure 1, the repulsive force acting on node m of the ownship UAS due to node n of the intruder aircraft is defined as

$$f_{rp}(m, n) = \begin{cases} \hat{\mathbf{d}}_{OI}(m, n)\gamma_{rp1}e^{(-\gamma_{rp2}\|\mathbf{d}_{OI}(m,n)\|)} & if\ |m - n| < k\ and \\ & \|\ \mathbf{d}_{OI}(m, n)\ \| < d_{max} \\ 0 & Otherwise, \end{cases} \tag{4}$$

where $\gamma_{rp1}, \gamma_{rp2}$ are nonnegative constants, d_{max} is the greatest distance over which nodes can influence each other, and k is a positive integer that determines the time dependence of the interactions. As we have no control over the intruder's chain, the ownship's path is pushed away from the intruder's path while the intruder's path is not influenced by the ownship's path.
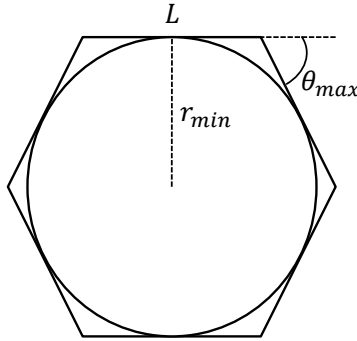
Merging all of the repulsive forces acting on the chain of the ownship by the chain of the intruder, we obtain

$$\mathbf{F}_{rpOI} = \left[F_{rpOI}^T(1),\ F_{rpOI}^T(2), \cdots, F_{rpOI}^T(N)\right]^T. \tag{5}$$

Where

$$F_{rpOI}(m) = \sum_{n=1}^{N} f_{rp}(m, n), \tag{6}$$

is the sum of all the forces acting on the mth node of the ownship by all the nodes of the intruder.

Figure 2. θ_{max}, the maximum allowable turn angle to approximate a circle using a discrete chain.

To be consistent with the kinematics of fixed wing aircraft, we introduce a straightening force that prevents the chain from violating the minimum turn radius of the UAS. Similar to 12, the applied force on any link that causes a turn is designed to ensure that $|\theta_i| < \theta_{max}$. As shown in Figure 2, θ_{max} is selected to ensure that

$$\theta_{max} < \frac{L}{r_{min}}, \tag{7}$$

American Institute of Aeronautics and Astronautics

and as Figure 3 shows, θ_i is the angle between $\mathbf{d}_{i1}$ and $\mathbf{d}_{i2}$, defined as

$$\theta_i = \arccos(\mathbf{d}_{i1}.\mathbf{d}_{i2}),$$

where $\mathbf{d}_{i1} = z_{N-1} - z_{N-2}$ and $\mathbf{d}_{i2} = z_{N-2} - z_{N-3}$, then the straightening force is defined as

$$\mathbf{f}_{st}(i) = \frac{\mu_i(\mathbf{d}_{i1})^\perp}{1 + \exp(k(\theta_{max} - \theta_i))}, \tag{8}$$

where $i = 1, 2, \ldots, N$, $\mu_i = (N + 1 - i)$ is the upper limit of the straightening force for node i, k is a positive constant that define how closely the logistic function approximates a step function and $(\mathbf{d}_{i1})^\perp$ is the orthogonal complement of $\mathbf{d}_{i1}$.
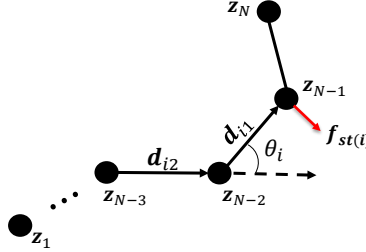
Figure 3. The straightening force applied to link N is designed to ensure that $|\theta_N| < \theta_{max}$.

Define $\mathbf{F}_{st} \triangleq \left[\mathbf{f}_{st}^T(1), \mathbf{f}_{st}^T(2), \ldots, \mathbf{f}_{st}^T(N)\right]^T$ to be the vector of all straightening forces applied to the chain and let $\mathbf{F}_{rw}$ be the reward force that is responsible for pushing the chain in the desired direction. Then the total unconstrained force $\mathbf{F}$ of system (1) is given by

$$\mathbf{F} = \mathbf{F}_{rw} + \mathbf{F}_{rpOI} + \mathbf{F}_{st}. \tag{9}$$

In addition, we want the motion of the link to be constrained by the kinematics of the chain, so that the distance between adjacent links is fixed as shown by Figure 4. Let L be the desired length of each link in the chain. These constraints can be written as

$$\| \mathbf{z}_2 - \mathbf{z}_1 \|^2 = L^2$$
$$\| \mathbf{z}_3 - \mathbf{z}_2 \|^2 = L^2$$
$$\vdots$$
$$\| \mathbf{z}_N - \mathbf{z}_{N-1} \|^2 = L^2,$$

or alternatively as

$$\phi(\mathbf{c}) \triangleq \begin{bmatrix} \| \mathbf{z}_2 - \mathbf{z}_1 \|^2 - L^2 \\ \| \mathbf{z}_3 - \mathbf{z}_2 \|^2 - L^2 \\ \vdots \\ \| \mathbf{z}_N - \mathbf{z}_{N-1} \|^2 - L^2 \end{bmatrix} = 0. \tag{10}$$

Differentiating the constraints once with respect to time results in the velocity constraint

$$\psi(\mathbf{c}) \triangleq \begin{bmatrix} 2(\mathbf{z}_2 - \mathbf{z}_1)^T(\dot{\mathbf{z}}_2 - \dot{\mathbf{z}}_1) \\ 2(\mathbf{z}_3 - \mathbf{z}_2)^T(\dot{\mathbf{z}}_3 - \dot{\mathbf{z}}_2) \\ \vdots \\ 2(\mathbf{z}_N - \mathbf{z}_{N-1})^T(\dot{\mathbf{z}}_N - \dot{\mathbf{z}}_{N-1}) \end{bmatrix} = 0. \tag{11}$$

Differentiating once more results in the acceleration constraint, which can be written in matrix notation as

$$\mathbf{A}(\mathbf{c})\ddot{\mathbf{c}} = \mathbf{b}(\dot{\mathbf{c}}), \tag{12}$$
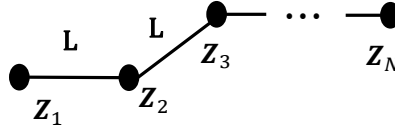
Figure 4. N-links chain.

where

$$\mathbf{A}(\mathbf{c}) \triangleq \begin{bmatrix} (\mathbf{z}_2 - \mathbf{z}_1)^T & 0 & \cdots & 0 \\ -(\mathbf{z}_3 - \mathbf{z}_2)^T & (\mathbf{z}_3 - \mathbf{z}_2)^T & \cdots & 0 \\ \vdots & \ddots & & \vdots \\ 0 & \cdots & -(\mathbf{z}_{N-2} - \mathbf{z}_{N-1})^T & (\mathbf{z}_{N-2} - \mathbf{z}_{N-1})^T \\ 0 & \cdots & 0 & -(\mathbf{z}_N - \mathbf{z}_{N-1})^T \end{bmatrix}, \tag{13}$$

and

$$\mathbf{b}(\dot{\mathbf{c}}) \triangleq - \begin{bmatrix} (\dot{\mathbf{z}}_2 - \dot{\mathbf{z}}_1)^T(\dot{\mathbf{z}}_2 - \dot{\mathbf{z}}_1) \\ (\dot{\mathbf{z}}_3 - \dot{\mathbf{z}}_2)^T(\dot{\mathbf{z}}_3 - \dot{\mathbf{z}}_2) \\ \vdots \\ (\dot{\mathbf{z}}_N - \dot{\mathbf{z}}_{N-1})^T(\dot{\mathbf{z}}_N - \dot{\mathbf{z}}_{N-1}) \end{bmatrix}. \tag{14}$$

The equation of motion of system (1) subject to constraints (12) is given by

$$\ddot{\mathbf{c}} = \mathbf{F} + \mathbf{A}^+(\mathbf{c})(\mathbf{b}(\dot{\mathbf{c}}) - \mathbf{A}(\mathbf{c})\mathbf{F}), \tag{15}$$

where $\mathbf{A}^+$ is the pseudo-inverse of $\mathbf{A}$.[15] As shown in 13, when solving equations of this type numerical error may cause the constraints $\phi(\mathbf{c})$ and $\psi(\mathbf{c})$ to drift from zero. Therefore, adding two additional terms forces the constrained accelerations to descend along the gradient of the constraints until they are no longer violated. Accordingly, Eq. (15) is modified as

$$\ddot{\mathbf{c}} = \mathbf{F} + \mathbf{A}^+(\mathbf{c})(\mathbf{b}(\dot{\mathbf{c}}) - \mathbf{A}(\mathbf{c})\mathbf{F}) - \gamma_p \frac{\partial \phi^T}{\partial \mathbf{c}}\phi - \gamma_v \frac{\partial \psi^T}{\partial \mathbf{c}}\psi, \tag{16}$$

where γ_p and γ_v are positive constants. A damping term is added to reduce oscillations and by combining the unconstrained force terms of eq. (9), eq. (15) becomes

$$\ddot{\mathbf{c}} = \mathbf{F}_{rw} + \mathbf{F}_{rpOI} + \mathbf{F}_{st} + \mathbf{A}^+(\mathbf{c})(\mathbf{b}(\dot{\mathbf{c}}) - \mathbf{A}(\mathbf{c})\mathbf{F})$$
$$- \gamma_p \frac{\partial \phi^T}{\partial \mathbf{c}}\phi - \gamma_v \frac{\partial \psi^T}{\partial \mathbf{c}}\psi + \gamma_d \dot{\mathbf{c}}. \tag{17}$$

In a similar way adopted by 12, when using the chain to avoid collisions in real-time, the first link serves as waypoint for the UAS to follow, and is not allowed to move. When the UAS nears the end of the first link, the link is removed from the chain and a new link is added to the end with the same direction as the last link in the chain. The first link that then comprise the beginning of the chain is fixed as new waypoint. So that the UAS always has an unchanging waypoint to follow while the remainder of the chain continuously adapts to changing virtual forces. One major advantage of this approach is that it can be extended to 3-D plane and then can be used to encounter for cases ascending or descending scenarios in the vinicity of airport.

## III.   Chain-Based Collision Avoidance with uncertainties

The collision avoidance algorithm presented in section II does not consider uncertainties associated with estimates of the intruder's states. In this section we develop a collision avoidance algorithm that takes into account the uncertainties of the estimates. We will assume that the estimated states of the intruder aircraft include both position and velocity. We also assume that an estimate of the accuracy of these state estimates is also provided and is quantified in an error covariance matrix. To take into account the

American Institute of Aeronautics and Astronautics

associated uncertainty with these estimates, a statistical distance is defined in lieu of the normal Euclidean distance computed between the intruder's chain nodes and the ownship's chain nodes. A Kalman Filter (KF) stage is introduced to the collision avoidance algorithm to receive the states estimate (position & velocity) and covariance at each time step from the 'sense' stage. The KF then propagates the state estimates and covariance N-steps into future, *where N is the number of chain nodes*, shown with solid red line in Figure 5. The intruder's chain nodes at $(t = T_1, t = T_2 \ldots t = T_N)$ represents an N-step position prediction of the intruder aircraft. At the next time step $(t = T_1)$, collision avoidance algorithm receives a new state estimate and covariance to update the the predicted intruder's location at $(t = T_1)$ and propagates the intruder's chain nodes at $(t = T_2, t = T_3 \ldots t = T_{N+1})$, shown with dashed green line. The N-link intruder chain is represented as

$$\mathbf{c}_I(k) = [\mathbf{z}_{I1}^T(k+1|k), \ \mathbf{z}_{I2}^T(k+2|k), \ldots, \mathbf{z}_{IN}^T(k+N|k)]^T,$$

where k is the time index, $(\cdot)(k)$ indicates the value of the state at time k and $(\cdot)(k+N|k)$ is the predicted value of the state at time $k+N$ given observations at time k. The associated covariance that represents the prediction uncertainty of each node is given by

$$\mathbf{Q}_I(k) = [Q_{I1}(k+1|k), \ Q_{I2}(k+2|k), \ldots, Q_{IN}(k+N|k)]^T,$$
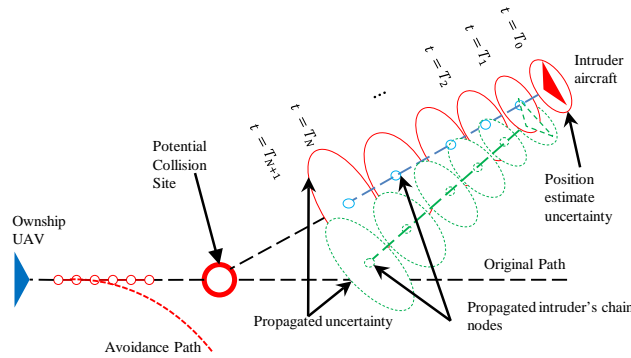
Figure 5. Intruder's chain Propagation.

Definition. The statistical distance or Mahalanobis distance between two points $x = (x_1, \ldots, x_p)^T$ and $y = (y_1, \ldots, y_p)^T$ in the p-dimensional space $\mathbb{R}_p$ is defined as

$$d_{\mathrm{M}}(x,y) = \sqrt{(x-y)^T Q^{-1}(x-y)}, \tag{18}$$

where Q is the covariance matrix that represents the measurement uncertainty of both variables x and y.[16, 17] $d_{\mathrm{M}}(x,0) = \|x\|_{\mathrm{M}} = \sqrt{x^T Q^{-1} x}$ is the Mahalanobis-norm (M-norm) of x.

The distance $\|\mathbf{d}_{OI}(m,n)\|_{\mathrm{M}}$ is then defined as

$$\|\mathbf{d}_{OI}(m,n)\|_{\mathrm{M}} = \sqrt{\left(\mathbf{z}_{Om} - \mathbf{z}_{In}(k+n|k)\right)^T Q_{In}^{-1}(k+n|k)\left(\mathbf{z}_{Om} - \mathbf{z}_{In}(k+n|k)\right)}. \tag{19}$$

To account for uncertainty in the estimate of the intruder's states, the repelling force given by Eq. (4) is replaced by

$$f_{rp}(m,n) = \begin{cases} \hat{\mathbf{d}}_{OI}(m,n)\gamma_{rp1}e^{(-\gamma_{rp2}\|\mathbf{d}_{OI}(m,n)\|_{\mathrm{M}})} & \textit{if } |m-n| < k \textit{ and} \\ & \|\mathbf{d}_{OI}(m,n)\| < d_{max} \\ 0 & \textit{Otherwise.} \end{cases} \tag{20}$$

IV. Collision Detection with Passive Sensor

As discussed in the introduction, one of the sub-functions of SAA is evaluating whether a detected aircraft is on a collision course. The problem of collision detection is related to the problem of signal detection and

estimation in the presence of noisy measurements. Many such problems reduce to hypotheses testing. The collision detection problem is also a special case of binary hypothesis testing where one of the hypothesis is that the intruder is on a collision course and the other is that it is on a safe course. For more details on signal detection and hypothesis testing, we refer to 18. With respect to aircraft conflict detection, many methods and frameworks have been previously proposed. A survey of 68 conflict detection and resolution methods is presented in 19. However, most of these approaches assume knowledge of the aircraft trajectory albeit with some uncertainty.

The current literature does not evaluate the collision detection performance that could be achieved by a specific sensing modality. Also missing is an evaluation of the system performance with realistic sensor noise and extensive Monte Carlo simulations to derive the False Alarm and Correct Detection rates of the proposed approaches. Sensors, such as electro-optical (EO) or infrared (IR) cameras, radars, and passive acoustics, can be used to detect non-cooperative intruders. EO sensors are particularly attractive because of their size, weight, and power (SWAP) characteristics, which are particularly relevant for small UAS applications. Apart from SWAP considerations, sensors such as radar cannot be used when operating close to the ground due to increased clutter and when flying in a hostile environment where radio signal silence is critical to the safety of the UAS platform and to the success of the mission.

Existing collision detection methods using passive sensors rely on computing the line-of-sight (LOS) rate of the intruder.[20] If the LOS rate of the intruder is nearly zero, then the intruder is considered on a collision course. Such a method suffers from high false alarm rate since faraway intruders usually yield small LOS rates, yet do not necessarily cause collision. In this section, we present a method for detecting imminent collisions using passive imaging sensors alone. Such a method is based on UtopiaCompression's unique technology – Monocular Maneuverless PAssive Ranging System (M2PARS), which estimates intruder's range and range rate with monocular passive sensors and without ownship maneuver.

A.   Monocular Maneuverless PAssive Ranging System (M2PARS)

Range estimation of the intruder using only a passive sensor can be formulated as a bearing-only tracking problem. The conditions of unobservability of the intruder aircraft in a bearing-only tracking problem have been extensively studied since the late 1970's.[21–25] This body of research has established that the intruder aircraft state is observable, in general, only if the order of the ownship dynamics is greater than the intruder dynamics. For an intruder moving with constant velocity, this implies that the sensor dynamics must involve an acceleration component. With the growing use of UASs in recent years, such a "maneuver-based" approach has been proposed as a solution to the EO based SAA problem for UASs: upon detecting an intruder, the UAS maneuvers in order to triangulate and resolve the position of the intruder.[26] However, a maneuver-based approach is undesirable in many ways. It may lead to waste of fuel, loss in mission performance, and is in general bad airmanship.

Funded by AFRL, UtopiaCompression Corporation (UC) developed M2PARS, a patent-pending approach to range estimation using passive monocular sensors with no ownship maneuver. M2PARS makes use of multiple image features to estimate intruder's state, include 3D position and velocity. UC has analytically proven the feasibility of M2PARS and has tested M2PARS using real flight test data [a].

B.   Collision detection logic and results

In this section, we discuss a simple collision detection logic similar to those presented in Reference 27. To be more specific, let the estimates of the intruder's position and velocity at time t be $p_{\text{int}}(t)$ and $v_{\text{int}}(t)$, respectively. Assume that the ownship's position and velocity from INS are known as $p_{\text{own}}(t)$ and $v_{\text{own}}(t)$. We further calculate the relative position and velocity between intruder and ownship as

$$p(t) = p_{\text{int}}(t) - p_{\text{own}}(t), \tag{21}$$
$$v(t) = v_{\text{int}}(t) - v_{\text{own}}(t). \tag{22}$$

Assume that the intruder moves with a constant velocity. Using $p(t)$ and $v(t)$, we predict the distance between the intruder and the ownship at time $t + \tau$ as

$$d(t + \tau) = \|p(t) + v(t)\tau\|. \tag{23}$$

---

[a]We refer interested readers to `http://www.utopiacompression.com/technologies/monocular_passive_ranging.php`

Define R_{safe} as the safe distance between intruder and ownship. That is, a collision occurs whenever the true range between intruder and ownship is less than R_{safe}. A non-collision encounter means that the true range between intruder and ownship is always greater than R_{safe}. To predict whether the collision will occur, we use the simple collision detection logic given in Algorithm 1.

Algorithm 1 Collision detection algorithm

1: **if** $\exists \tau \in (0, T]$ such that $d(t + \tau) < (1 + \delta) \times R_{\text{safe}}$ **then**
2:     collision detected
3: **else**
4:     no collision detected at time t
5: **end if**

In Algorithm 1, the parameters δ and T are positive real numbers and design parameters for the collision decision rule. The parameter T is the length of the prediction horizon. At any given time t, we check whether the intruder range is below the safe distance scaled by a factor of δ anytime within the next T seconds. Since there is always uncertainty associated with the estimates and the future maneuver of the intruder, we choose a non-zero δ to compensate for this uncertainty. We tune δ such that a desired correct detection rate and false alarm rate are achieved in simulation. To facilitate such tuning, we can perform Monte-Carlo simulations and plot the System Operative Characteristics (SOC) curve by varying δ. Assume that N simulations are performed, among which there are N_M true collision encounters. For a specific δ, Algorithm 1 detects $M(\delta)$ collision encounters, among which $C(\delta)$ encounters are the true collision encounters. Then we can calculate the correct detection rate (CDR) and false alarm rate (FAR) as

$$CDR = \frac{C(\delta)}{N_M}, \quad FAR = \frac{M(\delta) - C(\delta)}{N - N_M}. \tag{24}$$

By varying δ, we generate different CDR and FAR and plot them as the SOC curve. One can expect that as δ increases, both CDR and FAR will increase. Therefore, there exists a tradeoff between high CDR and low FAR. In the aircraft collision detection, we would like to detect all potential collisions, if possible. Thus, some false alarms will be expected. Our Monte Carlo simulations with constant velocity intruders have shown that we can achieve 95% CDR with 2% FAR using M2PARS and Algorithm 1. [b]

V.   Simulation Results

In order to test the effectiveness of the chain-based collision avoidance, we created a simulation consisting of 6-DOF model for both the ownship and the intruder, and we used the preliminary encounter geometry and Electro-Optical (EO) sensor based Passive Ranging collision detection model provided by UtopiaCompression Corporation (UC). The sensing model assumes 640×480 camera resolution, $48°$ camera field of view and frame rate at 30 fps. Two typical collision scenarios were employed to test the performance of the chain-based collision avoidance: approaching head-on and converging assuming the collision occurs when the d_{cpa} is less than 15 meters. A 10-link chain is chosen in both simulated scenarios.
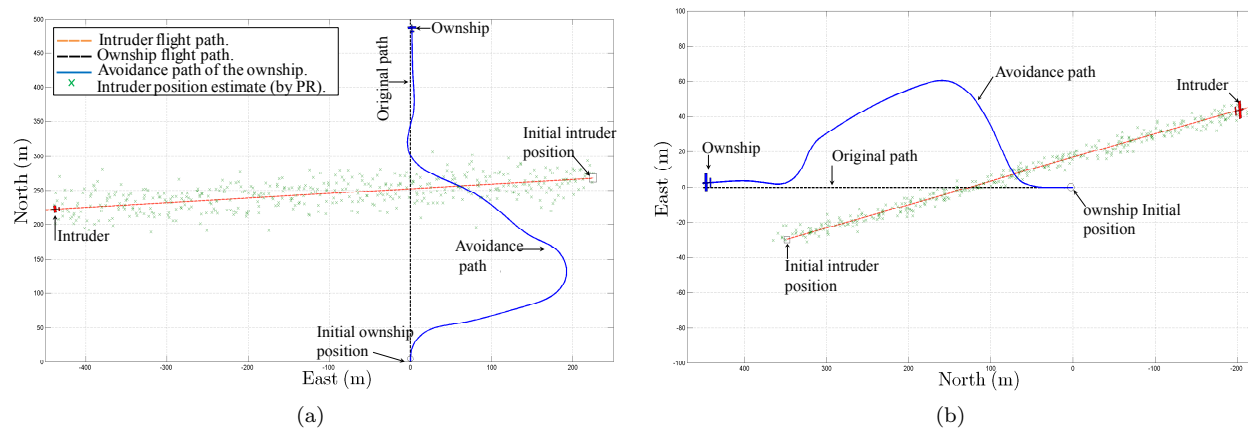

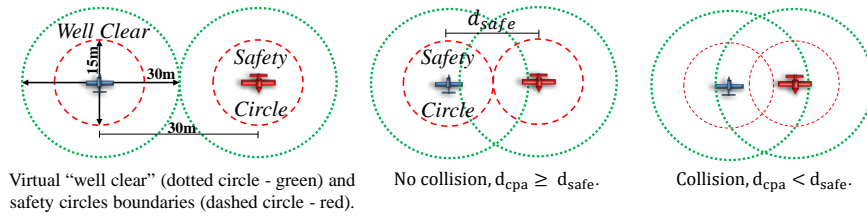(a)   (b)

Figure 6. Collision avoidance for the converging scenario (a) and the approaching head-on scenario (b).

---
[b]We refer interested readers to `http://www.utopiacompression.com/technologies/imminent_collision_detection.php`

Virtual "well clear" (dotted circle - green) and safety circles boundaries (dashed circle - red).

No collision, $d_{cpa} \geq d_{safe}$.

Collision, $d_{cpa} < d_{safe}$.

Figure 7. The well clear and safety circles boundaries. According to this defined geometry scheme, a collision occurs when the d_{cpa} is less than the safety distance, d_{safe}, which is set to 15 meters.

Figure 6 (a) shows the converging scenario. Note that the intruder has the right-of-way and the ownship should alter course to the right. The ownship initially starts from the origin in the inertial frame and follows a straight line. The initial range and bearing angle to the intruder is 349.49 meters and 49.92°, respectively and the d_{cpa}, if the collision avoidance algorithm is not initiated, is 8.20 meters. It is also assumed that the camera is rotated towards the right covering approximately 50° in azimuth in the inertial frame. Once the potential collision is detected and the range is less than the minimum allowable range, the ownship starts the collision avoidance strategy by implementing the chain-based algorithm causing the ownship to alter course to the right. We have assumed a constant velocity model for both the ownship and the intruder. The ownship had a cruising speed of 13 m/s and a minimum turn radius of 20 meters while the intruder speed is 15 m/s. For the head-on case, shown in Figure 6 (b) the initial range and bearing angle to the intruder is 350 meters and 94.88°, respectively and the d_{cpa} is 4.88 meters. Note that, both the ownship and intruder should alter course to the right. However, we have implemented the worst case scenario where the intruder violates the right-of-way rules and keeps moving in the same direction. The cruising speed of the ownship and the intruder for the approaching head-on scenario is 13 m/s and 15 m/s, respectively. Similar to the converging scenario, once the potential collision is detected and the range is less than the minimum allowable range, the chain-based collision avoidance algorithm is initiated to maneuver the ownship to the right and avoid an expected collision.

Covariance Pairs Index	1	2	3	4
Covariance Pairs: $[\sigma_{pn}, \sigma_{pe}]$, $[\sigma_{vn}, \sigma_{ve}]$	[0,0], [0,0]	[17.32,1.71], [2.45,0.18]	[34.66,3.42], [4.91,0.35]	[51.99,5.12], [7.36,0.53]

Figure 8. The uncertainty pairs of position and velocity estimates of the intruder. The subscripts *pn*, *pe* and *vn*, *ve* are position and velocity in north and east inertial coordinate frame, respectively.

We next use Monte Carlo simulation to investigate the level of performance that can be gained by using the chain based collision avoidance algorithm as the initial range to the intruder, initial bearing to the intruder and speed of the intruder varies provided that the uncertainty of the intruder position and velocity estimates also changes. Generally, any performance metric needs to take into account the competing objectives of collision avoidance logic, for instance preventing an imminent collision and minimizing deviation from flight-plan or waypoints path is two objectives that we will study. For the purpose of our simulation, and since the detection and avoidance logic will be implemented in the future using small UAS for both ownship and intruder, the radius of safety circle for both the ownship and the intruder is set to 7.5 meters so that the safe distance, d_{safe}, which is the sum of the radii of the ownship and intruder safety circles, is 15 meters. Thus, a collision occurs when d_{cpa} is less than 15 meters. In other words if the safety circles surrounding the ownship and the intruder intersect. The *well clear* boundary is set to 15 meters so that loss of self-separation occurs when d_{cpa} is less than 30 meters. Defining the *well clear* boundary does not mean that the current collision avoidance algorithm guarantees self-separation, but it is included solely as a reference parameter. Figure 7 depicts d_{safe}, *well clear* and collision boundaries. We have assumed that the ownship starts from the origin, with a 90° heading angle and a cruising speed of 13 m/s in all Monte Carlo simulations.

We defined a set of values for each one of the three chosen encounter geometry parameters, namely initial range to the intruder, initial bearing to the intruder and speed of the intruder. The Monte Carlo simulation starts with one of the three aforementioned parameters fixed for each value from the set the entire simulation run while other parameters are drawn from a uniform distribution derived from their nominal moments. At each given value from the set a hundred Monte Carlo trials is repeated for each pair of the uncertainty

American Institute of Aeronautics and Astronautics

where each trial runs the simulated collision avoidance scenario for 45 seconds. The four pairs of uncertainty associated with position and velocity estimates of the intruder are shown in Figure 8. The covariance matrix used in the Monte Carlo simulation using each pair of position and velocity is derived as

$$\mathbf{Q} = \begin{pmatrix} \mathbf{Q}_p & \mathbf{0} \\ \mathbf{0} & \mathbf{Q}_v \end{pmatrix}, \qquad \mathbf{Q}_p = \begin{pmatrix} \sigma_{pn}^2 & \sigma_{pn}\sigma_{pe} \\ \sigma_{pn}\sigma_{pe} & \sigma_{pe}^2 \end{pmatrix} \qquad \mathbf{Q}_v = \begin{pmatrix} \sigma_{vn}^2 & \sigma_{vn}\sigma_{ve} \\ \sigma_{vn}\sigma_{ve} & \sigma_{ve}^2 \end{pmatrix},$$

Repetitively, the Monte Carlo routine simulate a hundred trials for each value in the same set. Similarly, the Monte Carlo simulation is then repeated for each value of the next parameter's set having the other parameters drawn from a uniform distribution. The Monte Carlo simulated the same routine using both the approaching head-on and converging scenarios. A pseudo-code implementation of the Monte Carlo simulation is shown in Algorithm 2.
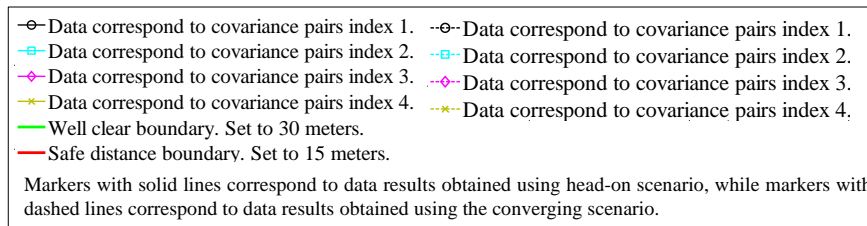

Figure 9. Legend for Figuers 10, 11 and 12

(a) Actual distance at the closest point of approach (CPA).

(b) Actual distance at the closest point of approach (CPA).

(c) Actual distance at the closest point of approach (CPA).

(d) Maximum deviation from waypoints path.

(e) Maximum deviation from waypoints path.

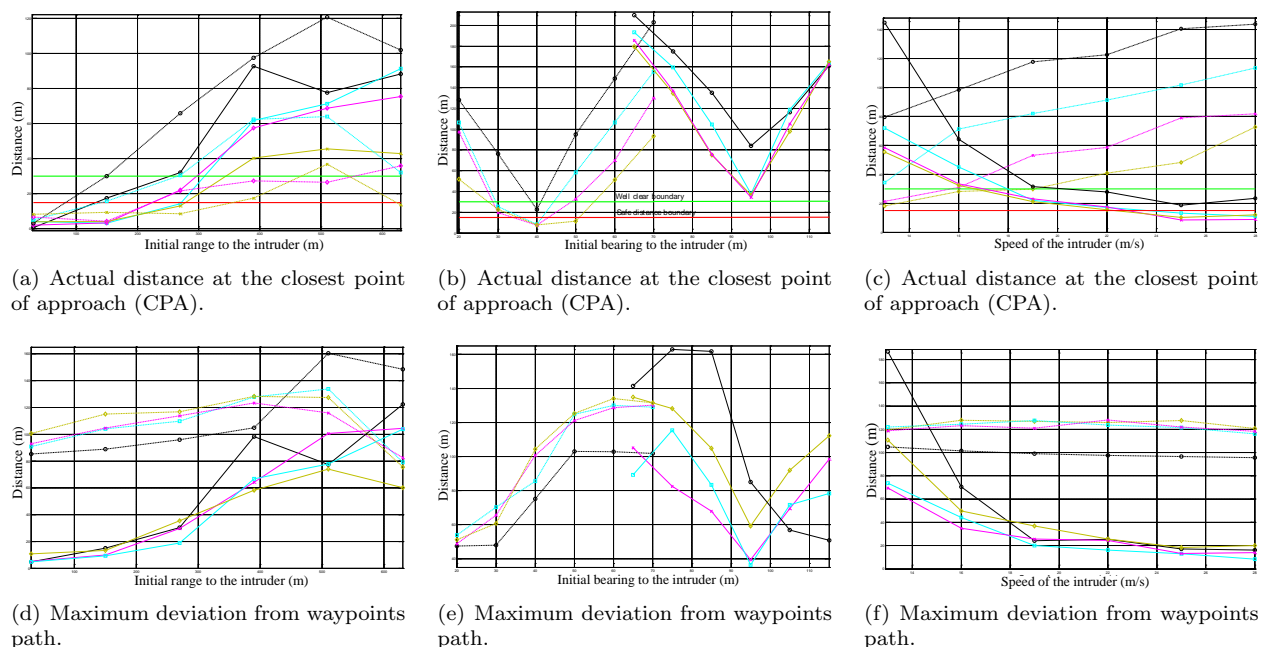(f) Maximum deviation from waypoints path.

Figure 10. Simulation results averaged for 100 Monte Carlo trials for different sets of initial range, bearing to the intruder and speed of intruder.

Figure 10 shows the results of the actual distance at the closest point of approach and the maximum deviation from waypoint path averaged over 100 Monte Carlo trials for each pair of uncertainty at each value of parameters set. The four different pairs of uncertainty are shown in four different colors while each parameter is shown in a separate figure. For instance, if we look at the actual distance at the closest point of approach results considering the head-on scenario, having initial range to the intruder is fixed at given each value of the set while other encounter geometry parameters drawn from a uniform distribution and covariance pair index 1, shown with solid black line in Figure 10(a), we noticed that the minimum required range to the intruder such that the chain based algorithm guarantee collision avoidance is 132

(a) Time required to run chain based collision avoidance algorithm code.

(b) Time required to run chain based collision avoidance algorithm code.

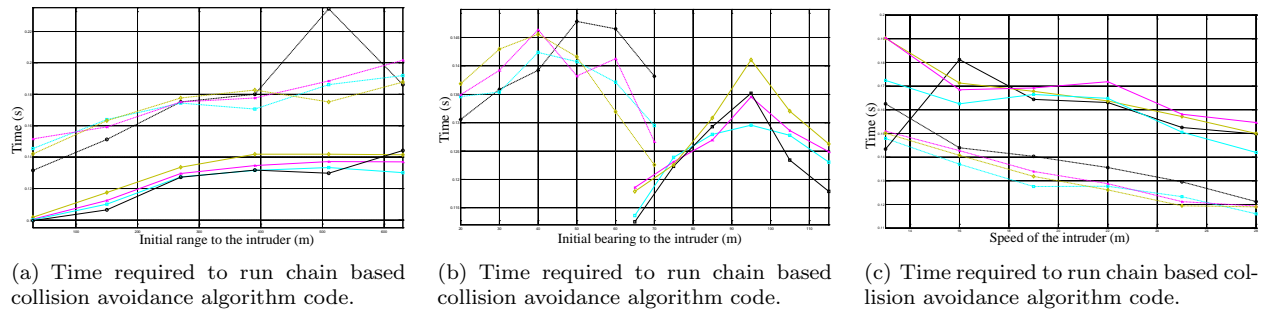(c) Time required to run chain based collision avoidance algorithm code.

Figure 11. Simulation results averaged for 100 Monte Carlo trials for different sets of initial range, bearing to the intruder and speed of intruder.
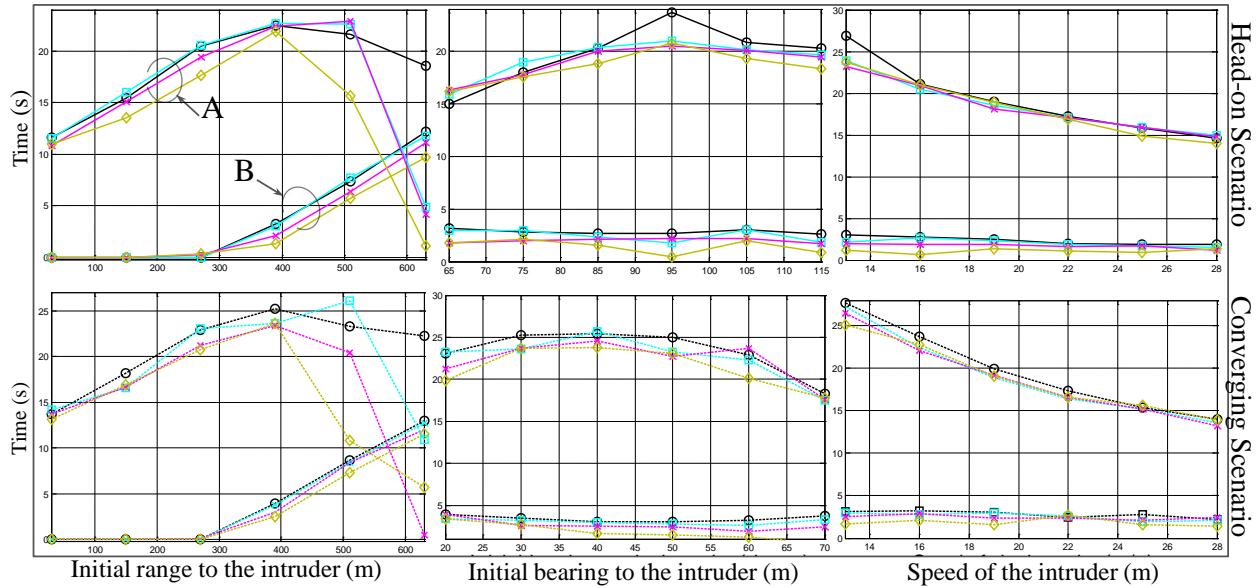

Figure 12. The time instant at which the chain based collision avoidance algorithm is initiated, curves with respect to each covariance pair tagged with (A), and the total time elapsed to accomplish the avoidance maneuver, curves with respect to each covariance pair tagged with (B).

meters. If we consider the next covariance pairs, covariance index 2, then the minimum range to the intruder should be at least 358 meters to guarantee collision avoidance. Figure 10(b) shows that in head-on scenario no matter is the initial bearing to the intruder given that the initial range to the intruder and speed of the intruder is within a certain ball about their nominal values then the chain based algorithm guarantee collision avoidance. Figure 10(c) shows that 23 m/s is the maximum speed of the intruder can have so that the algorithm guarantee collision avoidance considering head-on scenario and with respect to covariance pairs index 2, 3 and 4. On the other hand, we note that the actual distance at the closest point of approach in the converging scenario tend to increase as the speed of the intruder increases no matter what the uncertainty of intruder states is and that is because of the specific nature of this collision scenario geometry. As shown in Figures 11 and 12 the Monte Carlo simulations are also used to monitor the time instants at which the chain based collision avoidance algorithm is initiated and starts to maneuver the ownship to avoid an imminent collision, the time to accomplish the avoidance maneuver, and the time required to execute the chain based collision avoidance algorithm code during each iteration. We have defined the time required to accomplish the avoidance maneuver as the time difference between the time instant at which the chain based collision avoidance algorithm is activated and the time instant at which the range between the ownship and intruder is greater than the influence distance, which is set to 300 meters.

American Institute of Aeronautics and Astronautics

Algorithm 2 Monte Carlo Simulation Routine

1: **Define** :

   $rangeSet \triangleq [30, 150, 270, 390, 510, 630]$, $bearingSet_{sc1} \triangleq [20, 30, 40, 50, 60, 70]$, $bearingSet_{sc2} \triangleq [65, 75, 85, 95, 105, 115]$, $speedSet \triangleq [13, 16, 19, 22, 25, 28]$.

   $OwnshipStates \triangleq [Position, Speed, heading]$, $Position = [0, 0]$, $Speed = 13$, $heading = \gamma_O$.

   Nominal initial bearing: $InitialBearing_n = [49.92, 94.88]$.

   Nominal initial range: $Initial range_n = 350$. Nominal speed: $Speed_n = 15$, $Intruder heading \triangleq [\gamma_1, \gamma_2]$.

   $Intruder Postion = f(InitialBearing(Scenario), InitialRange)$.

   T_1 : Time instant at which algorithm is initiated , T_2: Time to accomplish the avoidance maneuver, T_3: Time required to execute the algorithm routine.

2: **for** $(Scenario = 1 \text{ to } 2)$ **do** {Converging and head-on scenarios abbreviated by sc1 and sc2, respectively.}

3:    **for** $(SetIndex = 1 : 6)$ **do**

4:       $InitialRange = rangeSet(SetIndex)$.

5:       **for** $(CovarianceIndex = 1 \text{ to } 4)$ **do** {Covariance pairs are shown in Figure 8}

6:          **for** $(MonteCarloTrial = 1 \text{ to } 100)$ **do**

7:             InitialBearing $= InitialBearing_n + U[a_\beta, b_\beta]$.

8:             IntruderSpeed $= Speed_n + U[a_{speed}, b_{speed}]$.

9:             $\mathbf{u} \triangleq [Intruder Postion, Intruder Speed, Intruder heading(Scenario), Ownship States]$.

10:            Input to the simulation model: $\mathbf{u}$.

11:            Run the corresponding collision avoidance Simulink model for 45 seconds.

12:            Output from the simulation model: $\mathbf{y} = [d_{cpa}, deviation from waypoit path, T_1, T_2, T_3]$.

13:          **end for**

14:       **end for**

15:    **end for**

16:    **if** (Scenario=1) **then**

17:       $bearingSet = bearingSet_{SC1}$.

18:    **else**

19:       $bearingSet = bearingSet_{SC2}$.

20:    **end if**

21:    **for** $(SetIndex = 1 : 6)$ **do**

22:       $Initial bearing = bearingSet(SetIndex)$.

23:       **for** $(CovarianceIndex = 1 \text{ to } 4)$ **do**

24:          **for** $(MonteCarloTrial = 1 \text{ to } 100)$ **do**

25:             InitialRange $= InitialRange_n + U[a_{range}, b_{range}]$.

26:             IntruderSpeed $= Speed_n + U[a_{speed}, b_{speed}]$.

27:             $\mathbf{u} \triangleq [Intruder Postion, Intruder Speed, Intruder heading(Scenario), Ownship States]$.

28:            Input to the simulation model: $\mathbf{u}$.

29:            Run the the corresponding collision avoidance Simulink model for 45 seconds.

30:            Output from the simulation model: $\mathbf{y}$.

31:          **end for**

32:       **end for**

33:    **end for**

34:    **for** $(SetIndex = 1 : 6)$ **do**

35:       $Intruder Speed = speedSet(SetIndex)$.

36:       **for** $(CovarianceIndex = 1 \text{ to } 4)$ **do**

37:          **for** $(MonteCarloTrial = 1 \text{ to } 100)$ **do**

38:             InitialBearing $= InitialBearing_n + U[a_\beta, b_\beta]$.

39:             IntruderSpeed $= Speed_n + U[a_{speed}, b_{speed}]$.

40:             $\mathbf{u} \triangleq [Intruder Postion, Intruder Speed, Intruder heading(Scenario), Ownship States]$.

41:            Input to the simulation model: $\mathbf{u}$.

42:            Run the the corresponding collision avoidance Simulink model for 45 seconds.

43:            Output from the simulation model: $\mathbf{y}$.

44:          **end for**

45:       **end for**

46:    **end for**

47: **end for**

American Institute of Aeronautics and Astronautics

VI. Conclusions and Future Work

In this paper, a feasible collision avoidance based on a virtual chain placed in a virtual force field is proposed. We have also presented a method for detecting imminent collisions using passive monocular sensors based on UtopiaCompression's unique technology M2PARS. The CA algorithm tries to find the proper evasive maneuver to avoid an expected collision with a detected intruder aircraft observing the FAA specified right-of-way rules. The chain based collision avoidance is advantageous because safe paths can be modified continuously as the underlying differential function changes, therefore there is no required amount of processing time to compute a flyable and safe paths.

We are currently working towards optimizing the number of links that represents the chain, as decreasing number of links reduces the required computational recourses to solve the underlying differential equations. On the other hand, improper selection of link number may cause the differential equations to become stiff and require more computational power. Another issue we would like to explore is to scale the chain based collision avoidance algorithm to act in scenarios where N-number of intruder aircrafts are detected. Future works also includes the implementation of this approach on our developed fixed wing airframes at the BYU MAGICC lab. The UASs that will be used in this effort are equipped with the Kestrel autopilot.

ACKNOWLEDGMENT

References

[1] Dalamagkidis, K., Valavanis, K., and Piegl, L. A., *On Integrating Unmanned Aircraft Systems into the National Airspace System*, Vol. 52, Springer Science+Business Media B.V. 2009, 2012, 2nd ed., 2012.

[2] R. H. Chen, A.Gevorkian, A. F. and Chen, W.-Z., "Multi-Sensor Data Integration for Autonomous Sense and Avoid," *American Institute of Aeronautics and Astronautics (AIAA)*, 2011.

[3] "Electronic Code of Federal Regulation (e-CFR)," [online] http://www.ecfr.gov.

[4] Sabatini, N., "Assuring the safe integration of UAS," *Unmanned Aircraft Systems: The Global Perspective*, 2007/2008.

[5] Weibel, R. E. and Hansman, R. J., "Safety Considerations For Operation Of Unmanned Aerial Vehicles In The National Airspace System," Tech. Rep. ICAT-2005-1, MIT International Center for Air Transportation, March 2005.

[6] Dalamagkidis, K., Valavanis, K., and Piegl, L., "Current Status and Future Perspectives for Unmanned Aircraft System Operations in the US," *Journal of Intelligent and Robotic Systems*, Vol. 52, 2008, pp. 313–329.

[7] Geyer, C., Singh, S., and Chamberlain, L., "Avoiding Collisions Between Aircraft: State of the Art and Requirements for UAVs operating in Civilian Airspace," *Carnegie Mellon University*, Jan 2008.

[8] Clothier, R., Palmer, J., Walker, R., and Fulton, N., "Definition of an airworthiness certification framework for civil unmanned aircraft systems," *Safety Science*, Vol. 49, 2011, pp. 871–885.

[9] 112th Congress, "FAA Modernization and Reform Act of 2012," H.R. 658, February 2012.

[10] Angelov, P., *Sense and Avoid in UAS: Research and Applications*, John Wiley & Sons, Ltd, 2012.

[11] *FAA Order 8700.1, Change 3, Chapter 169, section 5A*, Federal Aviation Administration.

[12] Argyle, M., Chamberlain, C., and Beard, R., "Chain-Based Path Planning for Multiple UAVs," *2011 50th IEEE Conference on Decision and Control and European Control Conference*, Orlando, FL, USA, December 2011.

[13] McLain, T. W. and Beard, R. W., "Trajectory Planning for Coordinated Rendezvous of Unmanned Air Vehicles," Vol. 2000-4369, American Institute of Aeronautics and Astronautics, Inc (AIAA), 2000.

[14] Chamberlain, C., *System Identification, State Estimation, and Control of Unmanned Aerial Robots*, Master's thesis, Department of Electrical and Computer Engineering, Brigham Young University, April 2011.

[15] Udwadia, F. and Kalaba, R., *Analytical Dynamics: A New Approach*, Cambridge University Press, 1996.

[16] Mahalanobis, P. C., "On the Generalised Distance in Statistics," *Proceedings of the National Institute of Sciences of India 2*, Vol. (1), 1936, pp. 49–55.

[17] Gnanadesikan, R. and Kettenring, J. R., "Robust Estimates, Residuals, and Outlier Detection with Multiresponse Data," *Biometrics*, Vol. 28, No. 1, Special Multivariate Issue, March 1972, pp. 81–124.

[18] Poor, H. V., *An Introduction to Signal Detection and Estimation*, Springer-Verlag, 2nd ed., 1994.

[19] Kuchar, J. K. and Yang, L. C., "A Review of Conflict Detection and Resolution Modeling Methods," *IEEE Transactions on Intelligent Transportation Systems*, Vol. 1, No. 4, December 2000, pp. 179–189.

[20] M.J. Kochenderfer, J. G. and Kuchar, J., "Hazard Alerting using Line-of-Sight Rate," *AIAA Guidance, Navigation and Control Conference and Exhibit*, Honolulu, Hawaii, 18 - 21 August 2008.

[21] Lindgren, A. and Gong, K., "Position and Velocity Estimation Via Bearing Observations," *IEEE Transactions on Aerospace and Electronic Systems*, Vol. 14, No. 4, July 1978, pp. 564–577.

[22] Nardone, S. C. and Aidala, V. J., "Observability Criteria For Bearings-Only Target Motion Analysis," *IEEE Transactions on Aerospace and Electronic Systems, AES*, Vol. 17, No. 2, March 1981, pp. 161–166.

[23]Aidala, V. and Hammel, S., "Utilization of Modified Polar Coordinates for Bearings-Only Tracking," *IEEE Transactions on Automatic Control*, Vol. 28, 1982, pp. 283–294,.

[24]Hammel, S. and Aidala, V. J., "Observability Requirements for Three-Dimensional Tracking via Angle Masurements," *IEEE Transactions on Aerospace and Electronic Systems*, Vol. 21, No. 2, March 1985, pp. 200–207.

[25]Payne, A., "Observability problem for bearings-only tracking," *International Journal of Control*, Vol. 49, 1989, pp. 761–76.

[26]O. Shakernia, W. C. and Raska, V., "Passive Ranging for UAV Sense and Avoid Applications," *Proceedings of the American Institute of Aeronautics and Astronautics Infotech*, AIAA, 2005.

[27]Ganguli, A. and Avadhanam, S., "On the Limits of Collision Detection Performance of a Sense-and-Avoid System for Non-Cooperative Air Traffic," *Proceedings of the AIAA Infotech Conference*, Atlanta, Georgia, April 2010.